Chapter 4

Bioconvectice hybrid stagnation-point flow due to induced magnetic field *

4.1 Introduction

The nanofluid studies involving microorganisms is an advancing field that has intrigued researchers due to its relevance in antibiotics, biofuel, toxin removal, targeted drug delivery and food digestion. The magnetic field represents an important characteristic of hydromagnetic problems. In some cases, the magnetic Reynolds number of the flow may not be realistic to be assumed small in magnitude; hence induced magnetic field (the additional magnetic field that gets induced on electrically conducting fluid in the presence of an external magnetic field.) is not negligible. However, studies incorporating induced magnetic field effects are limited in number. For its applications in biomedical imaging, hyperthermia, targeted drug delivery, and cancer therapy, the dynamics of water conveying single-wall carbon nanotubes (SWCNTs) and magnetite nanoparticles on the bioconvective stagnation-point flow along a stretching sheet subject to chemical reaction, viscous dissipation, induced magnetic field, and stratification effects is investigated. Relevant similarity formulas are effectuated in converting the governing equations into a system of ODEs and are further treated numerically using the Runge-Kutta-Fehlberg method with the shooting technique. Illustrations on the consequence of effectual parameters on the physical quantities and the flow profiles are achieved with the aid of graphs. The main objectives of the current chapter are to:

- Construct the bioconvective model to study the dynamics of water conveying

*Published in: International Communications in Heat and Mass Transfer (Elsevier), 2021; 126; 105484.

single-wall carbon nanotubes and magnetite nanoparticles considering induced magnetic field, thermal stratification, viscous dissipation, chemical reaction, solutal stratification, and motile density stratification effects.

- Provide theoretical knowledge on the consequence of effectual parameters on the flow profiles.
- Explore the significance of pertinent parameters on surface drag, heat transfer rate, mass transfer rate, and microorganism density number.

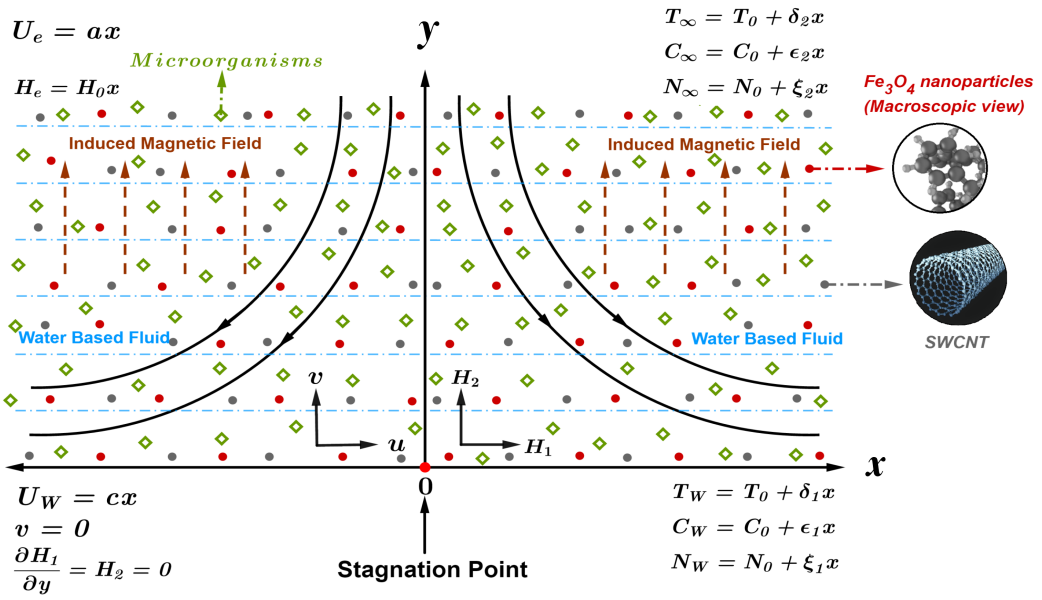

Figure 4.1: Geometrical Frame

4.2 Mathematical Frame

Two-dimensional steady incompressible stagnation point flow over a linearly elongating sheet (see Figure 4.1) is considered under the ensuing assumptions:

- The expanding sheet is positioned along x axis and water-based $Fe_3O_4 - SWCNT$ hybrid nanofluid (containing microorganisms) occupies the region $y > 0$.
- $U_W(x) = cx$ and $U_e(x) = ax$ correspond to the velocity of the lengthening sheet and the free stream, respectively.

- Induced magnetic field vector, $H = (H_1, H_2)$ is considered with H_1 & H_2 being the magnetic integrants along x and y direction, respectively.
- Chemical reaction and viscous dissipation effects are incorporated.
- Thermal, solutal and motile density stratification effects are also considered.

Following the aforementioned assumptions, the governing equations take the form (see Alsaedi et al., 2017; Z. Iqbal, Azhar, & Maraj, 2017):

$$\frac{\partial u}{\partial x} + \frac{\partial v}{\partial y} = 0 \tag{4.2.1}$$

$$\frac{\partial H_1}{\partial x} + \frac{\partial H_2}{\partial y} = 0 \tag{4.2.2}$$

$$u\frac{\partial u}{\partial x} + v\frac{\partial u}{\partial y} - \frac{\mu_e}{4\pi\rho_{hnf}}\left(H_1\frac{\partial H_1}{\partial x} + H_2\frac{\partial H_1}{\partial y}\right) = U_e\frac{dU_e}{dx} - \frac{\mu_e H_e}{4\pi\rho_{hnf}}\frac{dH_e}{dx} + \left(\frac{\mu_{hnf}}{\rho_{hnf}}\right)\frac{\partial^2 u}{\partial y^2} \tag{4.2.3}$$

$$u\frac{\partial H_1}{\partial x} + v\frac{\partial H_1}{\partial y} - H_1\frac{\partial u}{\partial x} - H_2\frac{\partial u}{\partial y} = \alpha_m\frac{\partial^2 H_1}{\partial y^2} \tag{4.2.4}$$

$$u\frac{\partial T}{\partial x} + v\frac{\partial T}{\partial y} = \alpha_{hnf}\frac{\partial^2 T}{\partial y^2} + \frac{\mu_{hnf}}{(\rho C_p)_{hnf}}\left(\frac{\partial u}{\partial y}\right)^2 \tag{4.2.5}$$

$$u\frac{\partial C}{\partial x} + v\frac{\partial C}{\partial y} = D_B\frac{\partial^2 C}{\partial y^2} - k_r\left(C - C_\infty\right) \tag{4.2.6}$$

$$u\frac{\partial N}{\partial x} + v\frac{\partial N}{\partial y} + \frac{bW_c}{C_W - C_0}\left(\frac{\partial}{\partial y}\left(N\frac{\partial C}{\partial y}\right)\right) = D_m\frac{\partial^2 N}{\partial y^2} \tag{4.2.7}$$

subject to the boundary conditions (see Alsaedi et al., 2017; Z. Iqbal, Azhar, & Maraj, 2017):

$$u = U_W(x) = cx,\ v = 0,\ \tfrac{\partial H_1}{\partial y} = H_2 = 0,\ T = T_W = T_0 + \delta_1 x,$$
$$C = C_W = C_0 + \epsilon_1 x,\ N = N_W = N_0 + \xi_1 x \quad \text{at } y = 0$$

$$u \to U_e(x) = ax,\ H_1 \to H_e(x) = H_0 x,\ T \to T_\infty = T_0 + \delta_2 x,$$
$$C \to C_\infty = C_0 + \epsilon_2 x,\ N \to N_\infty = N_0 + \xi_2 x \quad \text{as } y \to \infty$$

where $\alpha_m = \dfrac{1}{4\pi\mu_e\sigma_{hnf}}$ represents the magnetic diffusivity.

Consider the following similarity transformations (see Alsaedi et al., 2017; Z. Iqbal, Azhar, & Maraj, 2017):

$$u = cxf\,'(\zeta),\ v = -\sqrt{c\vartheta_f}f(\zeta),\ H_1 = H_0 x g\,'(\zeta),\ \zeta = y\sqrt{\frac{c}{\vartheta_f}},\ H_2 = -H_0\sqrt{\frac{\vartheta_f}{c}}g(\zeta),$$

$$\theta(\zeta) = \frac{T - T_\infty}{T_W - T_0},\ \psi(\zeta) = \frac{C - C_\infty}{C_W - C_0},\ \chi(\zeta) = \frac{N - N_\infty}{N_W - N_0}$$

Employing the similarity transformations into Equations (4.2.1) – (4.2.7), we get:

$$f\,''' - A_1\,A_2\left\{(f\,')^2 - f\,f\,'' - \frac{\beta}{A_2}\left\{(g\,')^2 - g\,g\,'' - 1\right\} - A^2\right\} = 0 \tag{4.2.8}$$

$$g\,''' - \frac{A_5}{\lambda}\{g\,f\,'' - f\,g\,''\} = 0 \tag{4.2.9}$$

$$\theta\,'' + \frac{A_3\,Pr}{A_4}\,f\,\theta\,' + \frac{Ec\,Pr}{A_1\,A_4}(f\,'')^2 = 0 \tag{4.2.10}$$

$$\psi\,'' + Le\,f\,\psi\,' - Kr\,Le\,\psi = 0 \tag{4.2.11}$$

$$\chi\,'' + Lb\,f\,\chi\,' - Pe\,\{(\chi + \Omega)\,\psi\,'' + \chi\,'\,\psi\,'\} = 0 \tag{4.2.12}$$

subject to the boundary conditions

$$f(\zeta) = 0,\quad f\,'(\zeta) = 1,\quad g(\zeta) = 0,\quad g\,''(\zeta) = 0,\quad \theta(\zeta) = 1 - S_1,$$
$$\psi(\zeta) = 1 - S_2,\quad \chi(\zeta) = 1 - S_3 \quad \text{when } \zeta = 0$$

$$f'(\zeta) \to A,\quad g\,'(\zeta) \to 1,\quad \theta(\zeta) \to 0,$$
$$\psi(\zeta) \to 0,\quad \chi(\zeta) \to 0 \quad \text{as } \zeta \to \infty$$

where the dimensionless parameters are given in appendix I.

The hybrid nanofluid models incorporated are (see Mabood, Ashwinkumar, & Sandeep, 2022; Sreedevi & Reddy, 2019):

$$\frac{\mu_{hnf}}{\mu_f} = \frac{1}{(1-\phi_{Fe_3O_4})^{2.5}\ (1-\phi_{SWCNT})^{2.5}} = \frac{1}{A_1}$$

$$\frac{\rho_{hnf}}{\rho_f} = (1-\phi_{SWCNT})\left\{(1-\phi_{Fe_3O_4}) + \frac{\rho_{Fe_3O_4}}{\rho_f}\ \phi_{Fe_3O_4}\right\} + \frac{\rho_{SWCNT}}{\rho_f}\ \phi_{SWCNT} = A_2$$

$$\frac{(\rho C_p)_{hnf}}{(\rho C_p)_f} = (1-\phi_{SWCNT})\left\{(1-\phi_{Fe_3O_4}) + \frac{(\rho C_p)_{Fe_3O_4}}{(\rho C_p)_f}\ \phi_{Fe_3O_4}\right\} + \frac{(\rho C_p)_{SWCNT}}{(\rho C_p)_f}\ \phi_{SWCNT} = A_3$$

$$\frac{k_{hnf}}{k_{bf}} = \frac{1-\phi_{SWCNT}+2\phi_{SWCNT}\left(\frac{k_{SWCNT}}{k_{SWCNT}-k_{bf}}\right) ln\left(\frac{k_{SWCNT}+k_{bf}}{2k_{bf}}\right)}{1-\phi_{SWCNT}+2\phi_{SWCNT}\left(\frac{k_{bf}}{k_{SWCNT}-k_{bf}}\right) ln\left(\frac{k_{SWCNT}+k_{bf}}{2k_{bf}}\right)}$$

$$\frac{k_{bf}}{k_f} = \frac{k_{Fe_3O_4}+2k_f-2\phi_{Fe_3O_4}\left(k_f-k_{Fe_3O_4}\right)}{k_{Fe_3O_4}+2k_f+\phi_{Fe_3O_4}\left(k_f-k_{Fe_3O_4}\right)}$$

$$\frac{\sigma_{hnf}}{\sigma_f} = 1 + \frac{3\left\{\frac{\phi_{Fe_3O_4}\sigma_{Fe_3O_4}+\phi_{SWCNT}\sigma_{SWCNT}}{\sigma_f} - \left(\phi_{Fe_3O_4}+\phi_{SWCNT}\right)\right\}}{2+\left\{\frac{\phi_{Fe_3O_4}\sigma_{Fe_3O_4}+\phi_{SWCNT}\sigma_{SWCNT}}{\left(\phi_{Fe_3O_4}+\phi_{SWCNT}\right)\sigma_f}\right\} - \left\{\frac{\phi_{Fe_3O_4}\sigma_{Fe_3O_4}+\phi_{SWCNT}\sigma_{SWCNT}}{\sigma_f} - \left(\phi_{Fe_3O_4}+\phi_{SWCNT}\right)\right\}}$$

$$A_4 = \frac{k_{hnf}}{k_f} = \frac{k_{hnf}}{k_{bf}} \times \frac{k_{bf}}{k_f},\ and\ A_5 = \frac{\sigma_{hnf}}{\sigma_f}$$

The physical quantities are given by (see Alsaedi et al., 2017; Z. Iqbal, Azhar, & Maraj, 2017; Mabood et al., 2022):

$$\text{Local drag coefficient} \quad : \quad Cf_x = \frac{\tau_\omega}{\rho_f\ (U_w)^2} = \frac{\mu_{hnf}\ \left.\frac{\partial u}{\partial y}\right|_{y=0}}{\rho_f\ (U_w)^2}$$

$$\Rightarrow\ Cf_x\ Re_x^{1/2} = \frac{f\ ''(0)}{A_1}$$

$$\text{Local Nusselt number} \quad : \quad Nu_x = \frac{x\ q_\omega}{k_f\ (T_w - T_0)} = \frac{-x\ k_{hnf}\ \left.\frac{\partial T}{\partial y}\right|_{y=0}}{k_f\ (T_w - T_0)}$$

$$\Rightarrow\ Nu_x\ Re_x^{-\ 1/2} = -A_4\ \theta\ '(0)$$

Local Sherwood number : $$Sh_x = \frac{x\ q_m}{D_B\ (C_w - C_0)} = \frac{-x\ D_B\ \left.\frac{\partial C}{\partial y}\right|_{y=0}}{D_B\ (C_w - C_0)}$$

$$\Rightarrow\ Sh_x\ Re_x^{-\ 1/2} = -\ \psi\,'(0)$$

Local motile density number : $$Nn_x = \frac{x\ q_n}{D_m\ (N_w - N_0)} = \frac{-x\ D_m\ \left.\frac{\partial N}{\partial y}\right|_{y=0}}{D_m\ (N_w - N_0)}$$

$$\Rightarrow\ Nn_x\ Re_x^{-\ 1/2} = -\ \chi\,'(0)$$

where $Re_x = \frac{xU_W}{\vartheta_f}$ is the local Reynold's number.

4.3 Numerical Frame & Validation

Equations (4.2.8) - (4.2.12) together with the boundary conditions shows a nonlinear nature and it seems to be difficult to find the closed-form or exact solution for the considered problem. Hence, the approximate solutions are computed numerically employing the Runge-Kutta-Fehlberg method cum shooting technique. This is accomplished by initially assuming:

$$\Upsilon_1 = f,\quad \Upsilon_2 = f\,',\quad \Upsilon_3 = f\,'',\quad \Upsilon_3{}' = f\,''',\quad \Upsilon_4 = g,\quad \Upsilon_5 = g\,',$$
$$\Upsilon_6 = g\,'',\quad \Upsilon_6{}' = g\,''',\quad \Upsilon_7 = \theta\,,\quad \Upsilon_8 = \theta\,',\quad \Upsilon_8{}' = \theta\,'',\quad \Upsilon_9 = \psi,$$
$$\Upsilon_{10} = \psi\,',\quad \Upsilon_{10}{}' = \psi\,'',\quad \Upsilon_{11} = \chi\,,\quad \Upsilon_{12} = \chi\,',\quad \Upsilon_{12}{}' = \chi\,''$$

The reduced system of the first-order ODE is given by:

$$\Upsilon_1{}' = \Upsilon_2\ ,\ \Upsilon_2{}' = \Upsilon_3\ ,$$

$$\Upsilon_3{}' = A_1\ A_2\ \left\{\ (\Upsilon_2)^2 - \Upsilon_1\ \Upsilon_3 - \frac{\beta}{A_2}\ \left\{(\Upsilon_5)^2 - \Upsilon_4\ \Upsilon_6 - 1\right\} - A^2\ \right\},$$

$$\Upsilon_4{}' = \Upsilon_5\ ,\ \Upsilon_5{}' = \Upsilon_6\ ,$$

$$\Upsilon_6{}' = \frac{A_5}{\lambda}\ \{\ \Upsilon_4\ \Upsilon_3 - \Upsilon_1\ \Upsilon_6\ \}\ ,$$

$$\Upsilon_7{}' = \Upsilon_8\ ,\ \Upsilon_8{}' = -\left\{\frac{A_3\ Pr}{A_4}\ \Upsilon_1\ \Upsilon_8 + \frac{Ec\ Pr}{A_1\ A_4}\ (\Upsilon_3)^2\right\},$$

$\Upsilon_9{}' = \Upsilon_{10}$, $\Upsilon_{10}{}' = Kr\ Le\ \Upsilon_9 - Le\ \Upsilon_1\ \Upsilon_{10}$,

$\Upsilon_{11}{}' = \Upsilon_{12}$, $\Upsilon_{12}{}' = Pe\ \left\{ (\Upsilon_{11} + \Omega)\ \Upsilon_{10}{}' + \Upsilon_{12}\ \Upsilon_{10} \right\} - Lb\ \Upsilon_1\ \Upsilon_{12}$.

with

$$\Upsilon_1(0) = 0, \quad \Upsilon_2(0) = 1, \quad \Upsilon_3(0) = \Gamma_1, \quad \Upsilon_4(0) = 0,$$
$$\Upsilon_5(0) = \Gamma_2, \quad \Upsilon_6(0) = 0, \quad \Upsilon_7(0) = 1 - S_1, \quad \Upsilon_8(0) = \Gamma_3,$$
$$\Upsilon_9(0) = 1 - S_2, \quad \Upsilon_{10}(0) = \Gamma_4, \quad \Upsilon_{11}(0) = 1 - S_3, \quad \Upsilon_{12}(0) = \Gamma_5$$

where Γ_1 , Γ_2 , Γ_3 , Γ_4 & Γ_5 are estimated using shooting technique with a suitable initial guess.

Accuracy of the code and the validation of the current problem have been accounted for through a restrictive comparison of the present work with prior published works Hayat et al., 2015, 2016; Iqbal, Azhar, et al., 2017 (showcased in Table 4.1 and a commendable agreement is noted.

Table 4.1: Comparison of drag coefficient $\left(Cf_x Re_x^{1/2}\right)$ with Hayat et al., 2015, 2016; Iqbal, Azhar, et al., 2017 for different A values when $\phi_{Fe_3O_4} = \phi_{SWCNT} = \beta = \lambda = 0$

A	$\boldsymbol{Cf_x Re_x^{1/2}}$			
	Iqbal et al., 2017	**Hayat et al., 2015**	**Hayat et al., 2016**	**Present study**
0.1	-0.969386	-0.96939	-0.96937	-0.969386
0.2	-0.918107	-0.91811	-0.91813	-0.918107
0.5	-0.667263	-0.66726	-0.66723	-0.667264
0.7	-0.433475	-0.43346	-0.43345	-0.433476
0.8	-0.299388	-0.29929	-0.29921	-0.299389
0.9	-0.154716	-0.15458	-0.1545471	-0.154717
1	0	0	0	0

4.4 Results & Discussion

The consequence of influential parameters on microbial concentration ($\chi(\zeta)$), velocity ($f'(\zeta)$), concentration ($\psi(\zeta)$), temperature ($\theta(\zeta)$) and induced magnetic field ($g'(\zeta)$) profiles are illustrated via Figures 4.2 - 4.15. Studies have been carried out for water-based $Fe_3O_4 - SWCNT$ hybrid nanofluid and Fe_3O_4 nanofluid with

Prandtl number (Pr) and infinity fixed at 6.2 and 10, respectively. Thermophysical properties of the conventional fluid (water), Fe_3O_4 (nanoparticle 1), and $SWCNT$ (nanoparticle 2) are showcased in Table 4.2.

Table 4.2: Thermophysical properties of water, Fe_3O_4 and $SWCNT$

Property	**Water** *(conventional fluid)*	**Fe_3O_4** *(nanoparticle 1)*	**SWCNT** *(nanoparticle 2)*
$\boldsymbol{\rho}$	997	5180	2600
$\boldsymbol{C_p}$	4179	670	425
$\boldsymbol{k}$	0.613	9.7	6600
$\boldsymbol{\sigma}$	0.05	25000	10^6

Figures 4.2(a) & 4.2(b) illustrate the impact of stretching parameter (A) on $f'(\zeta)$ & $g'(\zeta)$, respectively and it is perceived that augmenting A values produces a constructive effect on $f'(\zeta)$ and destructive effect on $g'(\zeta)$. Figure 4.3 depicts the variations in $f'(\zeta)$ due to β (magnetic parameter). It is observed that $f'(\zeta)$ increases for augmenting β values when $A < 1$ and a reversed behaviour is observed for $f'(\zeta)$ when $A > 1$.

Figure 4.4 bespeaks the deviation in $g'(\zeta)$ concerning β. An increase in $g'(\zeta)$ for $A < 1$ and a decrease $g'(\zeta)$ for $A > 1$ are noted for elevating β values. Figure 4.5 explains the mixed effect of λ (reciprocal of magnetic Prandtl number) on $g'(\zeta)$). Initially, elevating λ values decays $g'(\zeta)$ and afterwards, a reversed trend is observed when $A < 1$. A similar but inversed impact is perceived when $A > 1$.

Figures 4.6 & 4.7 elucidate the simultaneous effect of β, $\phi_{Fe_3O_4}$ & ϕ_{SWCNT} on $Cf_xRe_x^{1/2}$ (drag coefficient). It can be interpreted that $Cf_xRe_x^{1/2}$ improves with β and deteriorates with $\phi_{Fe_3O_4}$ & ϕ_{SWCNT} when $A < 1$. When $A > 1$, $Cf_xRe_x^{1/2}$ increases with $\phi_{Fe_3O_4}$ & ϕ_{SWCNT} and decreases with β. Biologically, a higher drag coefficient implies increased interaction between the fluid and the surface, which is beneficial in targeted drug delivery and biomedical imaging.

Variation in $\theta(\zeta)$ due to $\phi_{Fe_3O_4}$ (volume fraction of nanoparticle 1) and ϕ_{SWCNT} (volume fraction of nanoparticle 2) are illustrated in Figures 4.8(a) & 4.8(b), respectively. It is observed that $\theta(\zeta)$ ascends with augmenting $\phi_{Fe_3O_4}$ & ϕ_{SWCNT}. Physically, this increase in temperature can be related to the improvement in the

thermal conductivity of the nanoliquid caused by larger nanoparticle occupancy. The constructive effect of Ec (Eckert number) is illustrated in Figure 4.9(b). Physically, it is associated with the generation of friction forces between the fluid particles which increases the temperature profile. In addition, the analysis on the significance of $\phi_{Fe_3O_4}$, ϕ_{SWCNT} & Ec on the temperature profile unveils that the nanoliquid can be used for killing tumors or cancerous cells. Figure 4.9(a) depicts a descending nature of $\theta(\zeta)$ for S_1 (thermal stratification parameter). Physically, the decrease in the nanoliquid temperature is due to the decrease in the temperature difference between the surface and away from the surface caused by an increase in S_1.

The simultaneous effect of Ec, S_1, $\phi_{Fe_3O_4}$ & ϕ_{SWCNT} on $Nu_x Re_x^{-1/2}$ (heat transfer rate) has been studied with the aid of Figures 4.10 & 4.11. It can be said that for $A = 0.8$, $Nu_x Re_x^{-1/2}$ decreases with respect to S_1, Ec & ϕ_{SWCNT} and remains almost unchanged with respect to $\phi_{Fe_3O_4}$.

Figure 4.12 explains the consequence of Kr (chemical reaction parameter), Le (Lewis number) and S_2 (solutal stratification parameter) on $\psi(\zeta)$. A decreasing behaviour on the concentration profile is observed for augmenting Kr, Le & S_2 values. Physically, an increase in S_2 descends the concentration profile due to the decrease in the volumetric fraction between the surface and reference nanoparticles. Moreover, an increase in Kr consumes more nanoparticles and hence concentration decreases. Biologically, consumption of more nanoparticles is directly proportional to improved medication and biomedical imaging.

Figure 4.13 discusses the impact of Pe (Peclet number) and S_3 (motile density stratification parameter) on $\chi(\zeta)$. It is observed that the augmenting effectual parameter values tend to decrease $\chi(\zeta)$. Physically, an augmentation in S_3 decreases the concentration difference of microorganisms between the surface and away from the surface and hence the microbial concentration decreases.

Figures 4.14(a) & 4.15(a) bespeak the simultaneous variation of Le, Kr & S_2 on $Sh_x Re_x^{-1/2}$ (mass transfer rate) and Figures 4.14(b) & 4.15(b) depict the simultaneous variation of Lb (bioconvection Lewis number), Kr & S_3 on $Nn_x Re_x^{-1/2}$ (microorganism density number). It can be easily observed that $Sh_x Re_x^{-1/2}$ increases with Kr & Le and decreases due to S_2. Furthermore, it is also noted that $Nn_x Re_x^{-1/2}$ increases with Kr & Lb and decreases due to S_3.

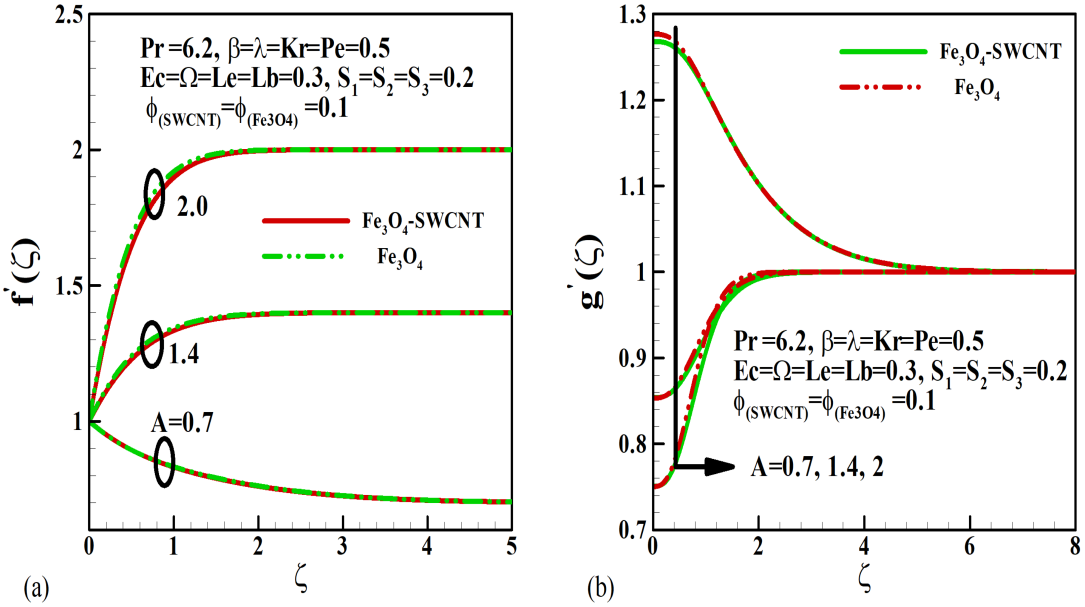

Figure 4.2: Variation of A on $f'(\zeta)$ & $g'(\zeta)$

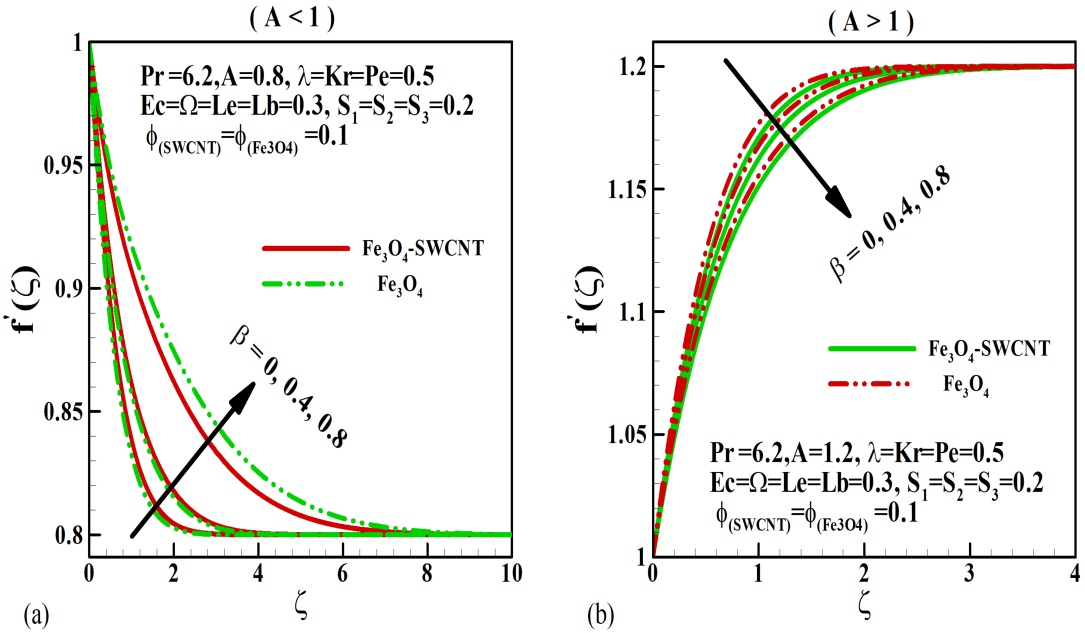

Figure 4.3: Variation of β on $f'(\zeta)$

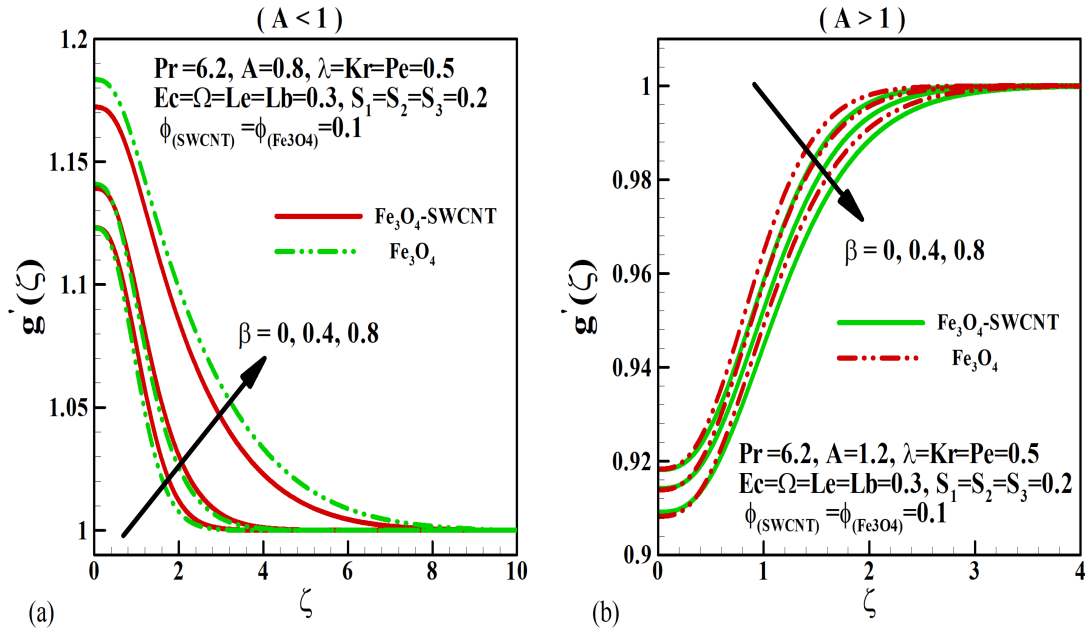

Figure 4.4: Variation of β on $g'(\zeta)$

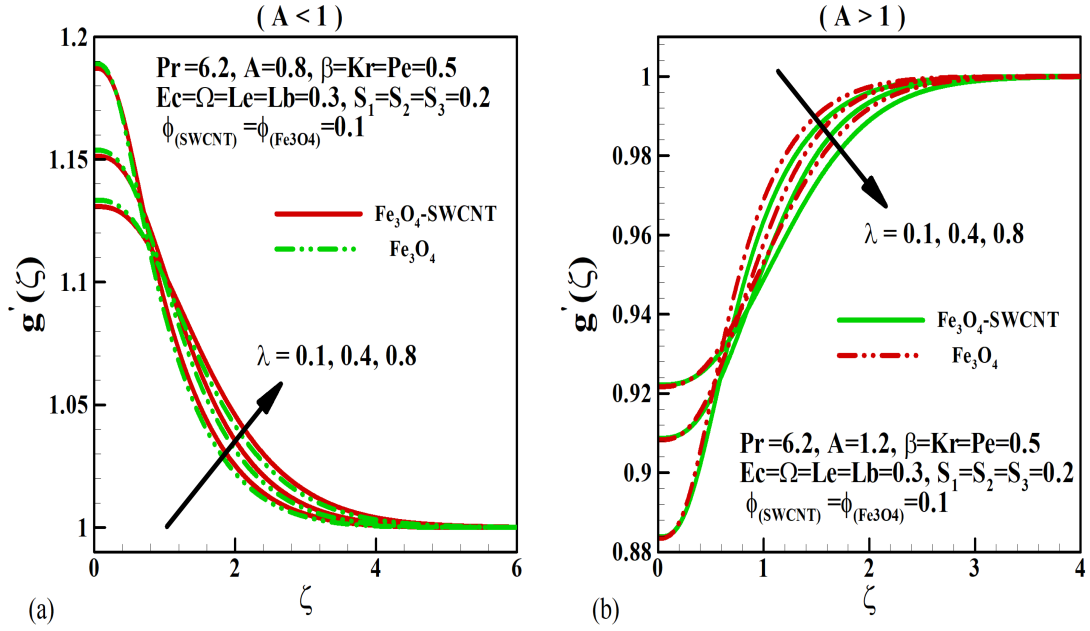

Figure 4.5: Variation of λ on $g'(\zeta)$

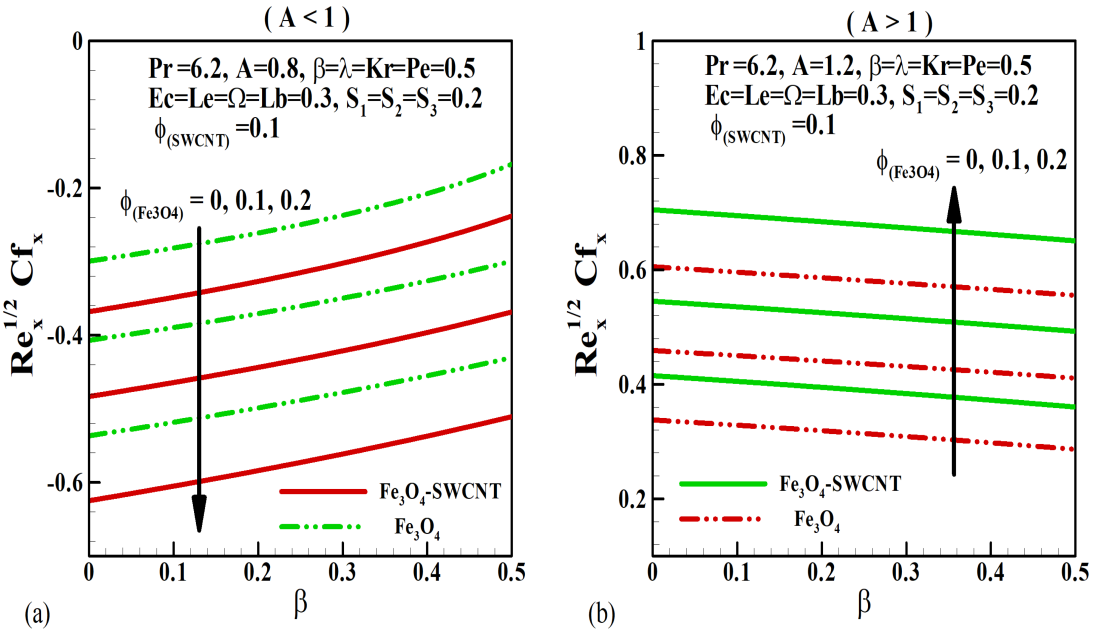

Figure 4.6: Parallel effect of β & $\phi_{Fe_3O_4}$ on $Cf_x Re_x^{1/2}$

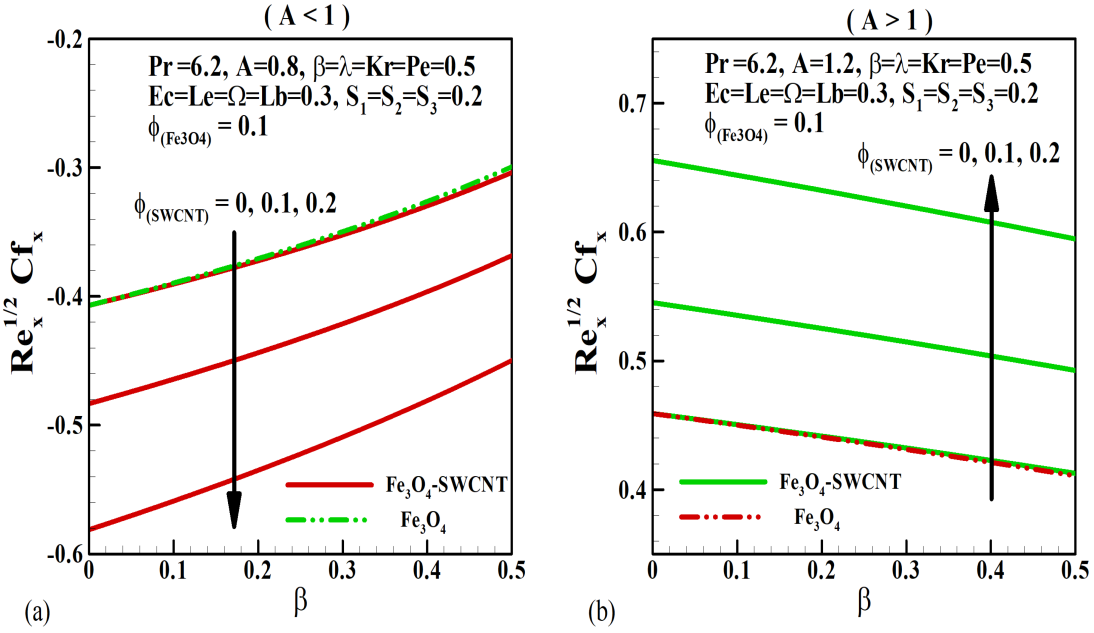

Figure 4.7: Parallel effect of β & ϕ_{SWCNT} on $Cf_x Re_x^{1/2}$

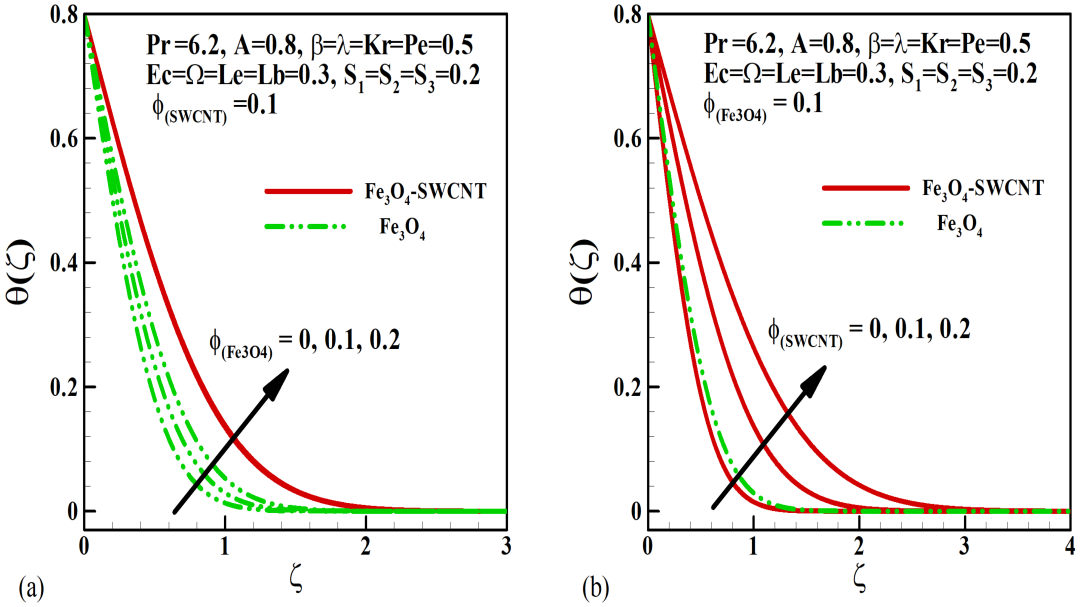

Figure 4.8: Variation of $\phi_{Fe_3O_4}$ & ϕ_{SWCNT} on $\theta\,(\zeta)$

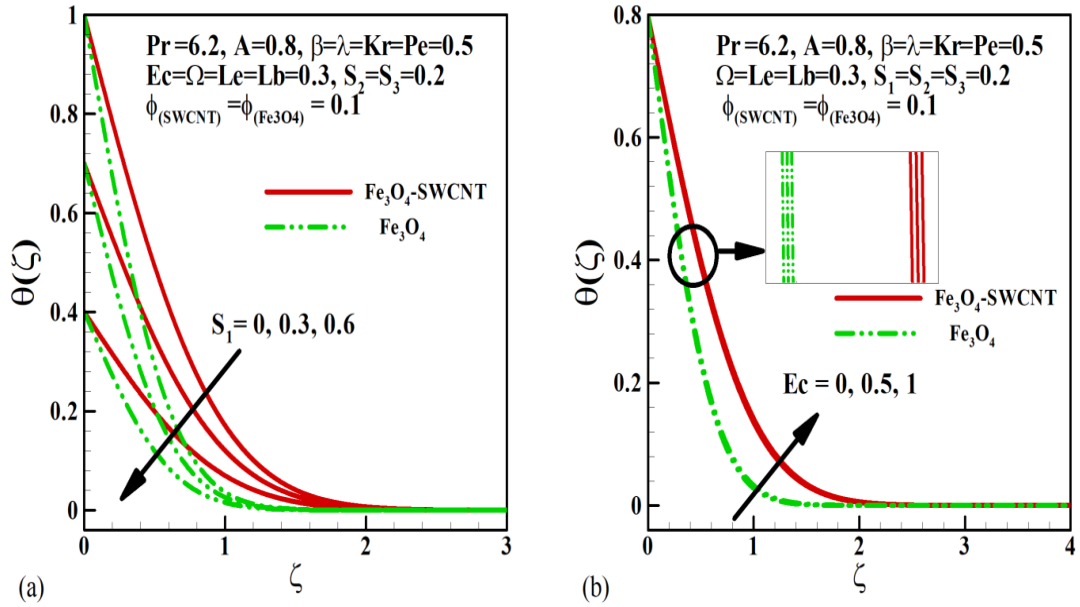

Figure 4.9: Variation of S_1 & Ec on $\theta\,(\zeta)$

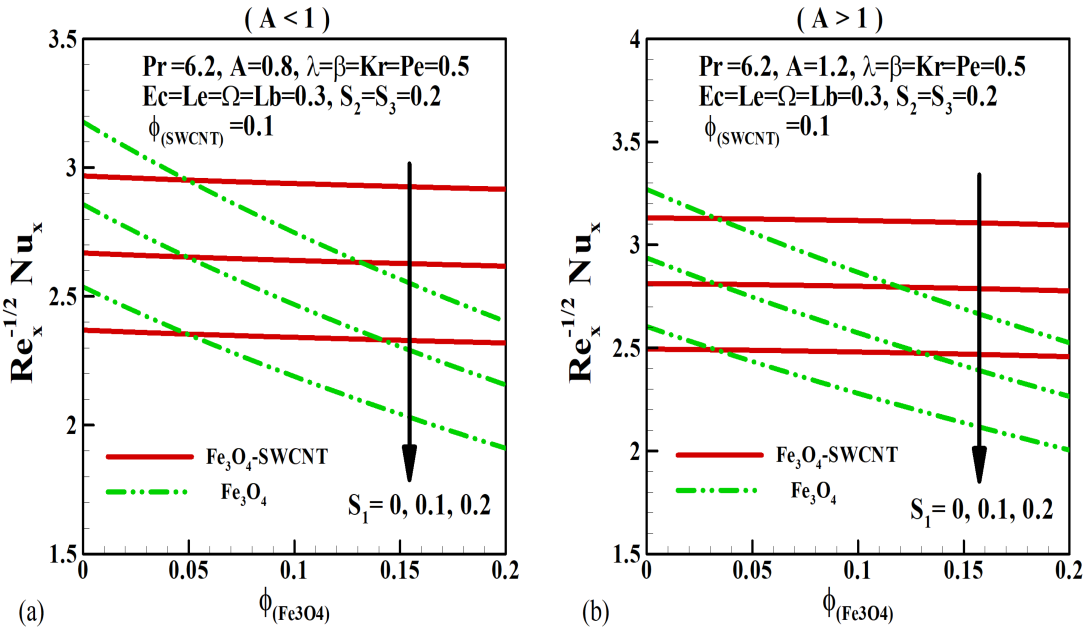

Figure 4.10: Parallel effect of S_1 & $\phi_{Fe_3O_4}$ on $Nu_x Re_x^{-1/2}$

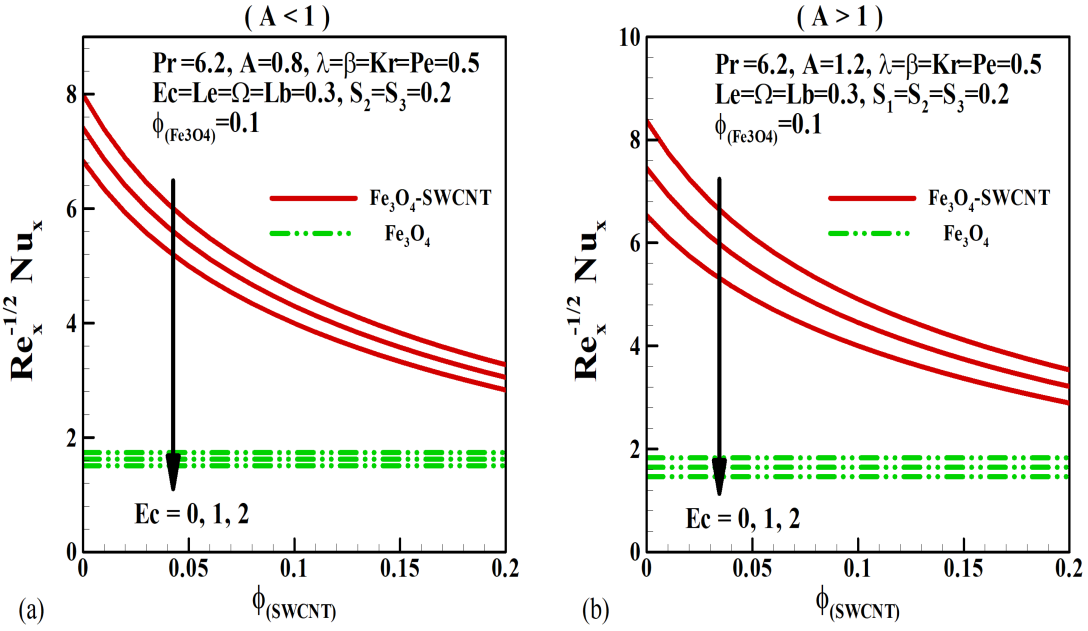

Figure 4.11: Parallel effect of Ec & ϕ_{SWCNT} on $Nu_x Re_x^{-1/2}$

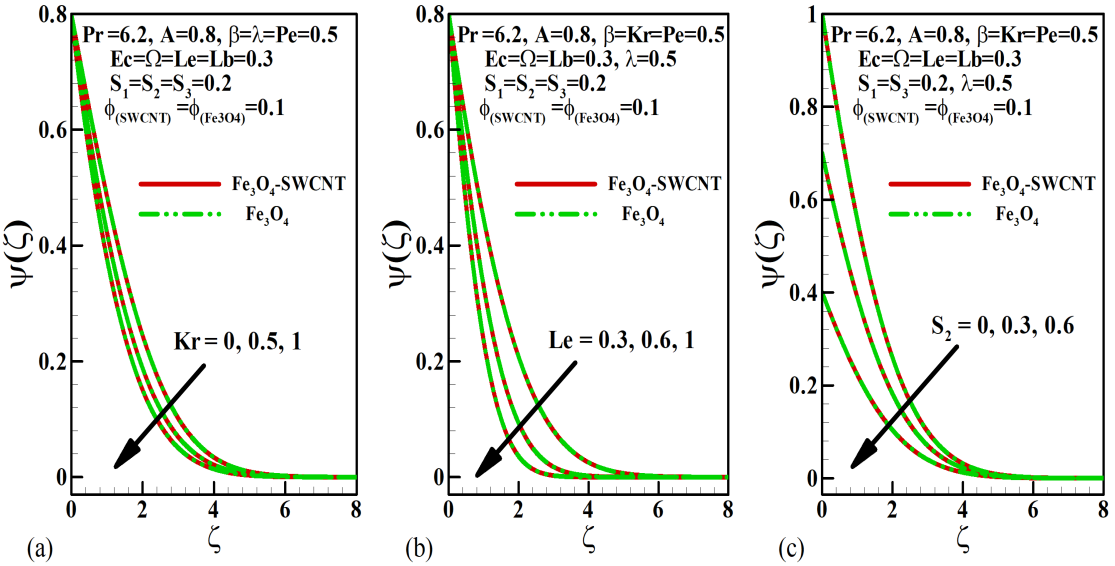

Figure 4.12: Variation of $Kr,\ Le,\ \&\ S_2$ on $\psi\,(\zeta)$

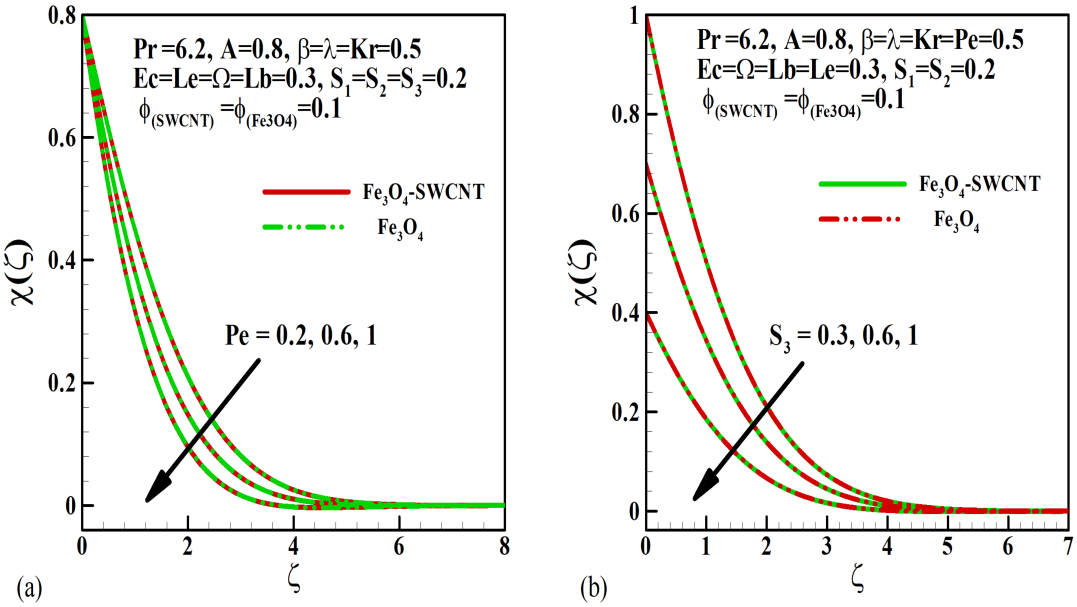

Figure 4.13: Variation of $Pe\ \&\ S_3$ on $\chi\,(\zeta)$

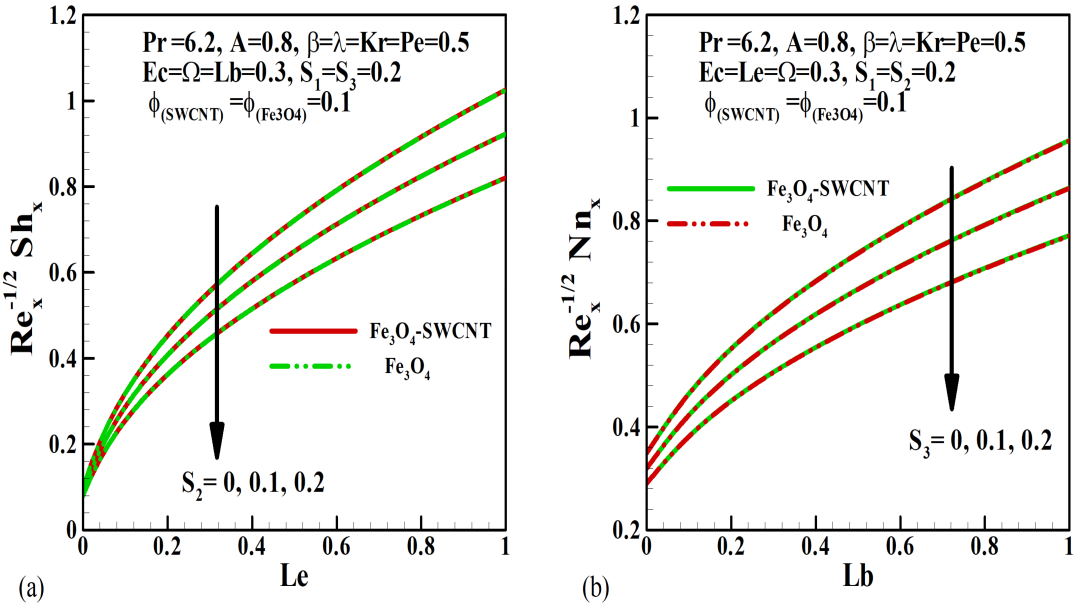

Figure 4.14: Parallel effect of (a) S_2 & Le on $Sh_x Re_x^{-1/2}$ and (b) S_3 & Lb on $Nn_x Re_x^{-1/2}$

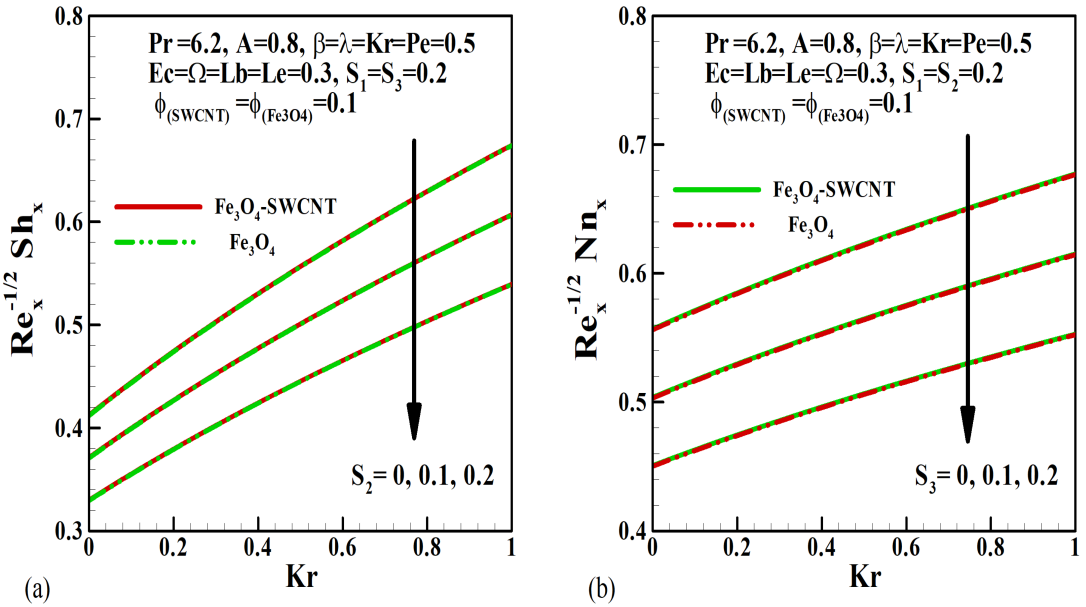

Figure 4.15: Parallel effect of (a) S_2 & Kr on $Sh_x Re_x^{-1/2}$ and (b) S_3 & Kr on $Nn_x Re_x^{-1/2}$

4.5 Conclusion

The dynamics of water conveying single-wall carbon nanotube and magnetite nanoparticles on the stagnation point flow along a stretching sheet subject to chemical reaction, viscous dissipation, induced magnetic field, and stratification effects have been numerically explored using the Runge-Kutta-Fehlberg method combined with the shooting technique. The key points noted from the study are:

- The augmenting volume fraction of single-wall carbon nanotube and magnetite nanoparticles raises the nanofluid temperature. Further, augmenting the Eckert number intensifies the nanofluid temperature. Biologically, the increase in the nanofluid temperature caused by the pertinent parameters is beneficial in killing tumors and cancerous cells.

- The velocity profile is directly proportional to the magnetic parameter when $A < 1$ and inversely proportional to the magnetic parameter when $A > 1$.

- The maximum drag coefficient (when $A = 0.8$) is experienced for higher values of the magnetic parameter and lower volume fraction of single-wall carbon nanotube and magnetite nanoparticles. However, the maximum drag coefficient (when $A = 1.2$) is experienced for lower values of the magnetic parameter and higher volume fraction of single-wall carbon nanotube and magnetite nanoparticles. Biologically, a higher drag coefficient implies increased interaction between the fluid and the surface, which is beneficial in targeted drug delivery and biomedical imaging.

- The mass transfer rate is a decreasing function of the solutal stratification parameter and an increasing function of the chemical reaction parameter.

- Augmenting chemical reaction parameter has a destructive effect on concentration profile that contributes towards improved medication and biomedical imaging.

- The maximum heat transfer rate is observed for smaller values of thermal stratification parameter, Eckert number, and nanoparticle volume fraction of single-wall carbon nanotube.

Appendix I: Non-dimensional qunatities

$A = \frac{a}{c}$	Stretching parameter
$\beta = \frac{\mu_e}{4\pi\rho_f}\left(\frac{H_0}{c}\right)^2$	Magnetic parameter
$\lambda = \frac{1}{4\pi\mu_e\sigma_f\vartheta_f}$	Reciprocal of magnetic Prandtl number
$Pr = \frac{(\mu C_p)_f}{k_f} = \frac{\vartheta_f}{\alpha_f}$	Prandtl number
$Kr = \frac{k_r}{c}$	Chemical reaction parameter
$Ec = \frac{(cx)^2}{(C_p)_f (T_W - T_0)}$	Eckert number
$Le = \frac{\vartheta_f}{D_B}$	Lewis number
$Lb = \frac{\vartheta_f}{D_m}$	Bioconvection Lewis number
$Pe = \frac{bW_c}{D_m}$	Bioconvection Peclet number
$\Omega = \frac{N_\infty}{N_W - N_0}$	Microorganism concentration difference parameter
$S_1 = \frac{\delta_2}{\delta_1}$	Thermal stratification parameter
$S_2 = \frac{\epsilon_2}{\epsilon_1}$	Solutal stratification parameter
$S_3 = \frac{\xi_2}{\xi_1}$	Motile density stratification parameter

Appendix II: Nomenclature

a, c	Dimensional constants	W_c	Maximum cell swimming speed
u, v	Velocity components	H_0	Uniform magnetic field at infinity
Nn_x	Local motile density	T_∞	Ambient fluid temperature
T_0	Reference temperature	N_∞	Ambient microbial concentration
C	Fluid concentration	C_0	Reference nanoparticle concentration
T	Fluid temperature	N_0	Reference microbial concentration
x, y	Cartesian coordinates	N_w	Microbial concentration near wall
b	Chemotaxis constant	C_w	Nanoparticle concentration near wall
T_w	Wall fluid temperature	C_∞	Ambient nanoparticle concentration
C_p	Specific heat	Cf_x	Local drag coefficient
k_r	Reaction rate constant	Nu_x	Local Nusselt number
Sh_x	Local Sherwood number	N	Microorganism concentration
σ	Electrical conductivity	H_e	Magnetic field at free stream
ζ	Dimensionless variable	D_B	Chemical molecular diffusivity
ϑ	Kinematic viscosity	D_m	Microorganism diffusion coefficient
k	Thermal conductivity	Ω	Microorganism concentration difference
μ_e	Magnetic permeability		parameter
ρ	Fluid density	λ	Reciprocal of magnetic Prandtl number
β	Magnetic parameter	ϕ	Nanoparticle volume fraction
α_m	Magnetic diffusivity	α	Thermal diffusivity